nuclear fusion IAEA

PAPER • OPEN ACCESS

Reconstruction of electromagnetic loads during disruptions in ITER

To cite this article: Fabio Villone *et al* 2026 *Nucl. Fusion* **66** 016030

OPEN ACCESS
IOP Publishing | International Atomic Energy Agency
Nuclear Fusion
Nucl. Fusion **66** (2026) 016030 (18pp)
https://doi.org/10.1088/1741-4326/ae1b1a

Reconstruction of electromagnetic loads during disruptions in ITER

Fabio Villone[1,*], Nicola Isernia[1], Guglielmo Rubinacci[1], Salvatore Ventre[2], Daniel Iglesias[3], Luis Maqueda[4], Daria Nikolaeva[3], Sergey Sadakov[3] and Álvaro Yáñez-González[4]

[1] DIETI/CREATE, Università degli Studi di Napoli Federico II, Via Claudio 21, 80125 Napoli, Italy
[2] DIEI/CREATE, Università degli Studi di Cassino e del Lazio Meridionale, Via Di Biasio 43, 03043 Cassino, (FR), Italy
[3] ITER Organization, Route de Vinon sur Verdon, CS 90 046, 12067 St. Paul les Durance, France
[4] Esteyco Mechanics, Avda. Burgos, 12B-Bajo, 28036 Madrid, Spain

E-mail: fabio.villone@unina.it

Received 14 March 2025, revised 6 October 2025
Accepted for publication 4 November 2025
Published 21 November 2025

Abstract
This paper presents a computational tool able to reconstruct electromagnetic (EM) loads due to disruptions in ITER. This will be one of the algorithms running in the 'Tokamak Systems Monitor', currently under development, whose main purpose is the evaluation of the overall behaviour of the ITER tokamak and its subsystems, by interpreting the available experimental data provided by engineering-oriented sensors. The input of the procedure consists of magnetic measurements (coil current measurements, discrete magnetic sensors, saddle loops, flux loops, Rogowski coils); the output is the EM (Lorentz) force density and its integrals (net force, moments) on the structures of interest. The procedure needs only a few minutes of computation on standard computer architecture, once all pre-computations have been carried out, hence it is suitable for inter-shot analysis. The same procedure can be in principle applied also to other fusion devices, provided that the required diagnostics is available.

Keywords: disruptions, electromagnetic loads, ITER

(Some figures may appear in colour only in the online journal)

1. Introduction

Tokamak devices are prone to disruptions [1], i.e. unexpected terminations of the plasma due to multiple causes, ranging from misfunctioning of control system, to the development of MHD instabilities, to the trespassing of operational thresholds for key physical quantities [2].

Although burning plasma devices will operate in regimes in which disruptions will be very unlikely, there will be always a chance of triggering a sequence of events that may lead to a disruption. As a consequence, disruptions can be considered as practically inevitable in tokamaks.

During a disruption, plasma magnetic and thermal energy is abruptly released, with potentially significant negative consequences on the structures surrounding the plasma. In particular, this can cause the melting of plasma-facing components and in addition it can generate electromagnetic (EM) loads on conductive components. Hence, the successful operation of future devices, like ITER, requires both improving the characterisation of disruption loads on existing devices and extrapolating them reliably to the scale of ITER and beyond [3]. In particular, the key strategy in ITER is to characterize disruption

[*] Author to whom any correspondence should be addressed.

loads at initial phases of operation, where the stored energy in the plasma is small and the risk of damage is lower.

The focus of the present paper is specifically on EM loads, that we briefly recall here.

The plasma evolution during a disruption goes through the following phases.

- *Vertical Displacement Event (VDE)*
  In case of loss of vertical position control, the plasma vertical position evolves exponentially in time, with a modest variation of plasma current due to magnetic flux conservation in a gradually deforming plasma. This phase might be absent in specific events like Major Disruptions.
- *Thermal Quench (TQ)*
  During this phase, the plasma thermal energy content is released on a time scale usually much faster than the typical EM time constants of the structures.
- *Current Quench (CQ)*
  After the Thermal Quench, the plasma resistivity increases significantly; consequently, the plasma current decreases, with a time dependence typically approximated as linear or exponential.

The modifications of the position and of the current of the plasma induce eddy currents in the surrounding conducting structures. In addition, after plasma-wall contact occurring during the VDE or at the TQ, currents may be injected directly from the plasma into the structures and vice-versa. These halo currents flow along open magnetic field lines in the scrape-off layer region of the plasma and close their path through the surrounding structures.

Hence, during a disruption, a current density will flow in the conducting structures, either induced (eddy currents) or injected (halo currents). The interaction of this current density $\mathbf{j}$ with the magnetic field $\mathbf{B}$ (both toroidal and poloidal) present in the device, gives rise to a Lorentz force density $\mathbf{j} \times \mathbf{B}$. This force density produces both local stress at given spatial locations and net EM loads (net vector force and moment) acting on specific components of the device. This is the electromagnetic load (EM load) that we will refer to in the following.

Experiments demonstrate that disruptions may exhibit some asymmetry in the toroidal direction. There are cases in which this effect cannot be neglected: the EM forces acting on various sectors of the vacuum vessel or the magnets, that would perfectly compensate in toroidally symmetric situations, in fact sum up to a non-zero value, so that opposite net horizontal lateral forces and moments at the vessel and the magnets appear. Such asymmetric EM interaction between the vessel and the magnets will not be addressed in the present paper.

Disruptions are hence a special concern for ITER. Also considering this, the 'Tokamak Systems Monitor (TSM)' is currently being developed by ITER Organization. Its main purpose is the interpretation of the ITER Tokamak Systems instrumentation, aimed at evaluating and understanding the overall behaviour of the ITER tokamak and the main parameters of its subsystems, during commissioning and operating states, including off-normal operation like disruptions. This interpretation will be compared by the tokamak operator with reference design values, allowing subsequent optimization of next experiments. Using available measurements, TSM will provide an integrated view of the overall hydraulic, thermal, structural and EM status of the main ITER systems (vacuum vessel, magnets, blankets, divertor, cryostat, thermal shields, diagnostics port plugs). Thanks to near-real-time processing, an online evaluation of the Tokamak systems status will be possible, with a latency of seconds or minutes. The online calculation capabilities will be expanded through offline data assessment, aimed at in-depth detailed analysis after the plasma discharges. Eventually, the TSM will contribute to find an optimal trade-off between tokamak performance and equipment lifetime.

In the framework of the TSM, several specific reconstruction algorithms have been developed, with the aim of estimating the actual loads acting on the internal components, starting from the measured experimental data during ITER operation. Previous work has been addressed to the development of reconstruction algorithms based on mechanical measurements [4] and to the set-up of three-dimensional computational models for the calculation of EM loads during symmetrical and asymmetrical disruptions [5, 6].

This paper presents a procedure able to reconstruct the EM loads acting on selected structures of interest of ITER, using only magnetic measurements as inputs. This procedure uses sensors which are independent from those used in [4], so the two approaches are completely complementary. Hence, during ITER operation they will be used for cross-calibration and mutual validation. The proposed procedure goes beyond other methods [7, 8], which are aimed at estimating only EM loads acting globally rather than on specific components.

The paper is organized as follows. Section 2 reports the methodology adopted, while section 3 presents the test cases analysed. Section 4 is focused on a critical discussion of the results obtained and section 5 draws the conclusions and outlines future work.

2. Methodology

The EM reconstruction procedure must satisfy a number of high-level requirements.

(a) *Only magnetic measurements will be used as inputs*
We will assume as inputs the following quantities, collectively referred to as 'magnetic measurements': coil currents (Central Solenoid, CS; Poloidal Field coils, PF coils; Toroidal Field coils, TF coils); magnetic sensors (discrete sensors, flux loops, saddle loops); Rogowski coils (around straps providing electrical connections).

(b) *The procedure will be run intershot*
The computations required to carry out the EM reconstruction procedure should only last a few minutes on a standard computational environment, once all suitable matrices have been precomputed.

(c) *The procedure must be modular and flexible*
The routines should be tuneable, in terms of parameters and settings. It should be possible to incorporate in the same framework and choose different computational models performing the same sub-task. There should be the possibility of using model libraries with different levels of accuracy.
(d) *Additional information should be easily incorporated*
The EM reconstruction procedure should be self-consistent on the one hand, but on the other it should be open to using eventually additional information, whenever possible or available, with the aim of improving the overall performances.
(e) *The procedure must be adaptable to available measurements*
Magnetic and non-magnetic measurements might become unavailable or unusable during operation; the EM reconstruction procedure must be able to adapt to this evolving situation.

In order to fulfil these high-level requirements, the architecture of the EM reconstruction procedure consists of two steps, as detailed in figure 1 and in the following.

2.1. STEP 1: EM identification

Using only magnetic measurements as inputs, the aim of this step is to identify currents flowing in structures where it cannot be measured directly (most notably the Vacuum Vessel, VV). STEP 1 consists of the following main sub-steps.

2.1.1. Plasma current and position identification.

The aim of this sub-step is to estimate the plasma current and centroid position, starting from the signals provided by the magnetic sensors. Let us call γ a closed line circumventing the plasma and no other toroidal current density. We suppose to know the magnetic field and the magnetic flux difference at a number of discrete locations along. From the knowledge of these quantities, we can estimate the plasma current and centroid position, as detailed in the appendix, resorting to a fairly standard procedure. In ITER, we can choose as line γ the position of the inner tangential magnetic sensors (set AA, 24 sensors in the poloidal plane), which practically coincides also with the position of the normal inner magnetic sensors (set AB) and of the flux saddle coils (set AD, 22 sensors in the poloidal plane) (figure 2). This line does not circumvent the currents flowing in the vessel, although it circumvents the blankets, which might alter the result, as it will be commented below.

2.1.2. Estimate of magnetic field due to unknown sources.

Once the plasma current and centroid position have been identified, a so-called 'tracker' converts these data to a number of axisymmetric filaments located in the poloidal plane, which are switched on and off at each time instant according to their proximity to the centroid. This mapping can be carried out incorporating different pieces of information and assumptions. Currently (figure 3), a regular grid of 2974 filaments has been considered, equally spaced of 10 cm in radial and vertical position. At each time instant, the nearest 10 filaments to the centroid are activated to represent the plasma, with a current distribution inversely proportional to distance from the centroid, with currents which sum up to the total estimated plasma current.

Describing the plasma with a relatively small set of filaments, spatially concentrated around the plasma centroid, introduces an approximation of the magnetic field produced by the plasma. We would like to point out that this approximation is similar to what is routinely done in plasma control, when resorting to so-called filamentary models, which successfully represent the EM interaction of the plasma with the surrounding structures by using one or few filaments around the plasma centroid [9].

Similarly, also the CS and the PF coils (including the in-vessel coils for vertical position control) can be described by a suitable number of axisymmetric filaments, carrying a current which is uniformly distributed over the poloidal cross-section of the coil. The number of filaments is chosen so as to have approximately the same number of filaments per square meter for all the coils.

Once both the plasma and the CS/PF coils have been represented by a number of filaments, their (purely poloidal) magnetic field B_{coils} and B_{plasma} can be estimated using Biot-Savart integral, at each spatial location and in particular where the magnetic sensors are located. Subtracting these contributions from the total magnetic field B available at magnetic sensors location, the magnetic field due to unknown sources (most notably the vacuum vessel) at sensors locations can be estimated as:

$$B_{\text{VV}} = B - (B_{\text{coils}} + B_{\text{plasma}}) .$$

The same reasoning obviously applies to flux loops and saddle loops.

2.1.3. Identification of unknown currents.

Using the estimation at magnetic sensors location of the magnetic field due to unknown sources currents only, it is possible to identify such currents via a suitable inversion technique. It should be noted that the sensors used in this part of the procedure are not only those located inside the vacuum vessel, used in section 2.1.1, but include virtually all the magnetic sensors of ITER, which are located both inside and outside the vessel. The computational tool presented in this paper is currently being updated to keep track of the latest version of the ITER magnetic sensor database.

Different choices are possible to carry out this inversion. If magnetic sensors were available both inside and outside each shell of the vessel, adopting a thin wall approximation, it would be possible to estimate the current density flowing in the vessel from the jump of the tangential component of the magnetic field. In the present paper, we use instead a singular value decomposition of the Biot-Savart matrix. In particular, we give a simplified representation of the geometry of the unknown sources (the vacuum vessel), as depicted in figure 4, featuring 110 current strips of finite width directed toroidally, neglecting

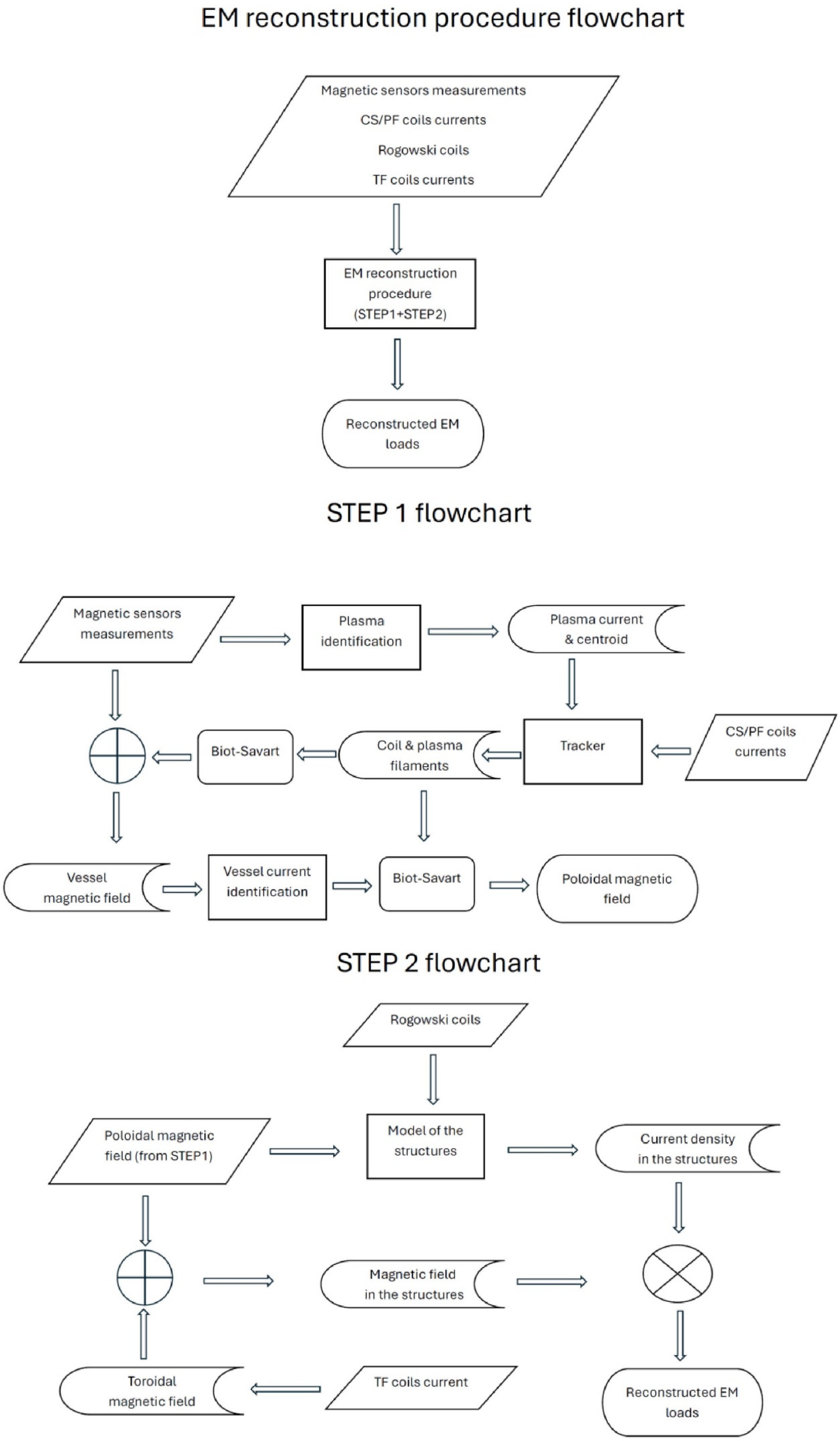

Figure 1. Overall architecture of the EM reconstruction procedure and breakdown in two steps.

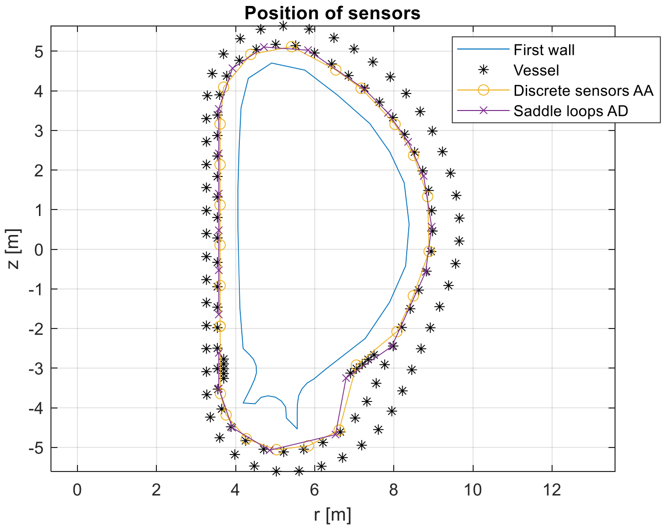

Figure 2. Location of magnetic sensors used for plasma identification in ITER.

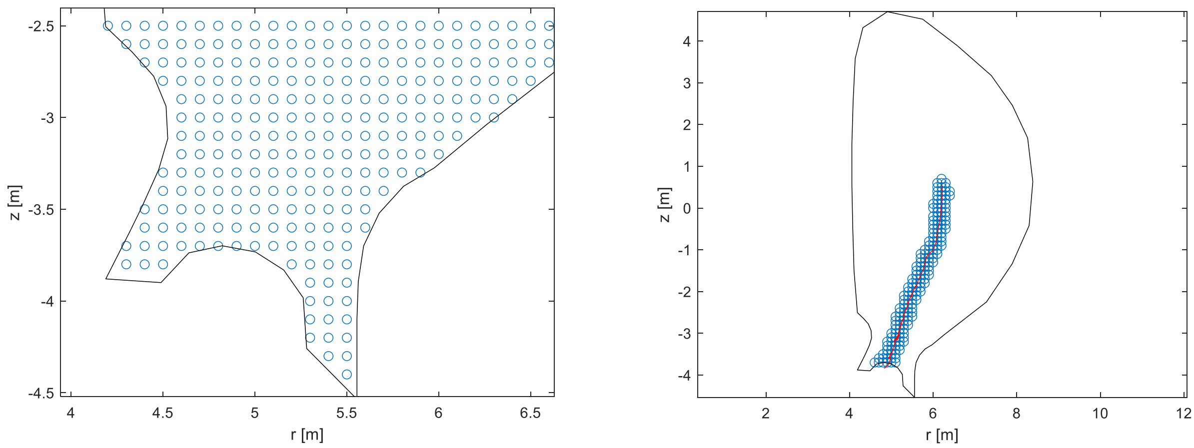

Figure 3. Regular grid of filaments used for representing the plasma and sample result of tracking procedure, showing the filaments activated around the centroid during one specific event.

all 3D features such as ports and blankets. Similarly, we neglect the poloidal current flowing in the vessel and its small effect on the toroidal field. We explicitly notice that this simplified description of the vessel is not used for the calculation of EM loads, which is treated in section 2.2 below. Rather, it is used to estimate the value of currents induced in the vessel by all other sources and the corresponding magnetic field. This means that all these simplifications (specifically, neglecting poloidal current and 3D features) do no impact directly the quality of EM load reconstruction.

We compute the matrix Q relating the currents flowing in these structures I_{VV} to the magnetic field at magnetic sensors location B_{vv} (the same reasoning applies to flux loops and saddle loops):

$$B_{\mathrm{VV}} = QI_{\mathrm{VV}}.$$

Then, we give a Singular Value Decomposition (SVD) of matrix Q as:

$$Q = USV^T$$

where S is a diagonal matrix of the same dimension as Q and with nonnegative diagonal elements (singular values), and U, V are unitary matrices, i.e. such that their inverse coincides with their transpose. Let us call n_r the number of singular values that we decide the retain in the inversion and let us define the reduced matrices:

$$U_{\mathrm{rid}} = U(:, 1:n_r),$$

$$V_{\mathrm{rid}} = V(:, 1:n_r),$$

$$S_{\mathrm{rid}} = S(1:n_r, 1:n_r).$$

We have:

$$B_{\mathrm{VV}} = QI_{\mathrm{VV}} = USV^T I_{\mathrm{VV}} \cong U_{\mathrm{rid}} S_{\mathrm{rid}} V_{\mathrm{rid}}^T I_{\mathrm{VV}}.$$

Posing $I_{\mathrm{VV}} = V_{\mathrm{rid}}\alpha$ and using the properties of unitary matrices, we have:

$$U_{\mathrm{rid}}^T B_{\mathrm{vv}} = U_{\mathrm{rid}}^T USV^T I_{\mathrm{VV}} = U_{\mathrm{rid}}^T USV^T V_{\mathrm{rid}}\alpha \cong S_{\mathrm{rid}}\ \alpha$$

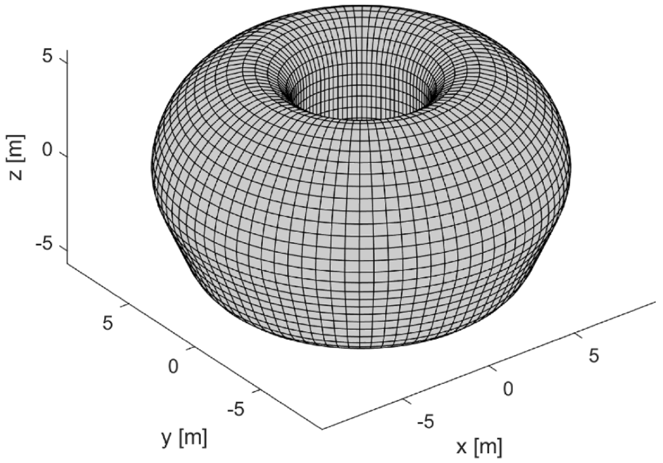

Figure 4. Simplified representation of the unknown sources (vacuum vessel). The toroidal strips are electrically insulated in the poloidal direction and cover both the inner and the outer vessel shells.

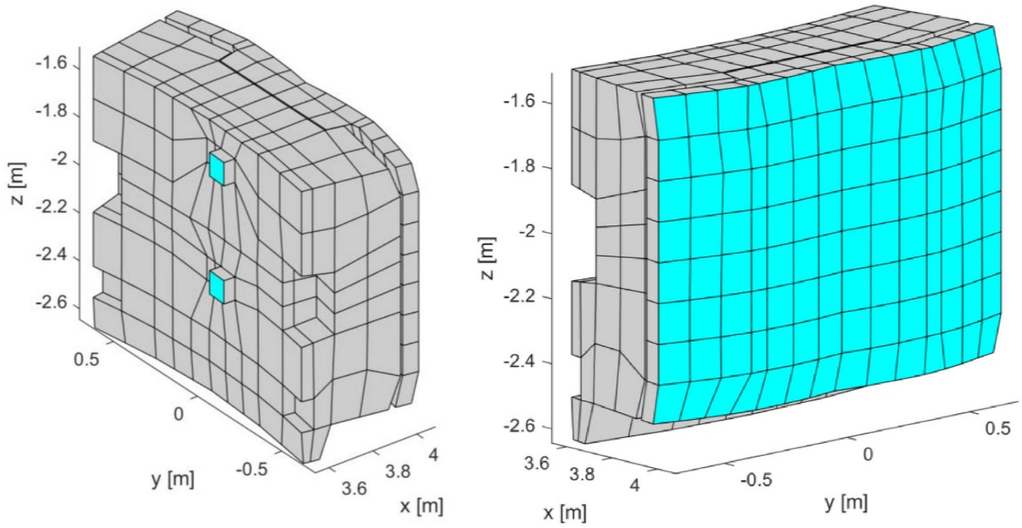

Figure 5. Example of Structure of Interest for the reconstruction of EM loads: ITER blanket module#1.

$$I_{\mathrm{VV}} = V_{\mathrm{rid}}\alpha \cong V_{\mathrm{rid}} S_{\mathrm{rid}}^{-1} U_{\mathrm{rid}}^{T}\, B_{\mathrm{VV}}.$$

This expression provides the identified values of the unknown sources I_{VV} as a function of their estimated magnetic field B_{VV}. Since it is well known that such inverse problems is ill-posed, in order to suitably regularize it, in the present application of the procedure, a small number of singular values (<10) has been retained in the identification procedure, which is carried out on top of the initially estimated value of the vessel currents. Once these unknown currents have been identified, the corresponding magnetic field can be computed at each spatial location (not only those corresponding to magnetic sensors) with Biot-Savart integrals. With the present simplifying assumption about the vessel description, also this magnetic field is purely poloidal; in more general cases, it may also have a toroidal component.

It should be noted that the procedure can easily adapt to the possible (temporary or permanent) unavailability of specific magnetic sensors. If some sensors cannot be used for any reason, it is necessary to eliminate some rows from the matrix Q and recompute the singular value decomposition.

2.2. STEP 2: EM loads reconstruction

Using the results of STEP 1 and a simplified model of the Structures of Interest (SoI in the following), the goal of this step is to estimate the EM loads acting on the SoI.

It is possible to build different models of the SoI, trading off accuracy and computational time. It is also possible to build separate models of each part of the structures, or all the SoI simultaneously. In the reminder of this section, we focus on one specific blanket module for exemplification, but the same reasoning obviously applies to any structure. A rather coarse geometrical description has been considered (figure 5), in order to have a short computational time. The volumetric elements are reported in grey, while cyan denotes the electrodes allowing a current flow (plasma facing components and straps connecting to vessel) [10].

2.2.1. Estimate of current density in the SoI. It is supposed that Rogowski coils are placed around the straps connecting the blanket module to the vacuum vessel, hence providing a measurement of the current I_{Rog} flowing in each of the straps—there are two such straps for the blanket under analysis. The sum of the two Rogowski coils measurements obviously provide the total halo current injected in the blanket module, through the front panel facing the plasma, while their difference provides the net current flowing in the blanket in the poloidal direction, which is included in the computatation, since it is important for the correct reconstruction of EM loads. Indeed, in [11, 12] it is demonstrated that erroneusly excluding the poloidal current may lead to completely different results and wrong quantifications of EM loads.

It is further supposed that the halo current is injected uniformly over the first wall of each single blanket module, so that each electrode of the first wall of each module is fed with an injected current I_{halo} which is a fraction of the total halo current of the module, according to its area as compared to the overall section. Consequently, since each blanket module experiences a different halo current, ranging from positive to negative values according to the actual flow of current from the plasma to the structures or vice-versa, the injected halo current density varies along the poloidal direction as a piecewise constant function.

In view of the estimate of their current density $\boldsymbol{J}_{\mathrm{SoI}}$, the SoI are represented by an integral formulation of the Magneto-Quasi-Static problem discretized in terms of edge-elements, in the stream of [13], so that $\boldsymbol{J}_{\mathrm{SoI}}$ can be described by a set of discrete variables I_{SoI} obeying the following equation:

$$L_{\mathrm{SoI}}\frac{dI_{\mathrm{SoI}}}{dt}+R_{\mathrm{SoI}}I_{\mathrm{SoI}}=V_{\mathrm{ext}}+F_{\mathrm{Rog}}\phi_{\mathrm{Rog}}+F_{\mathrm{halo}}\phi_{\mathrm{halo}}$$

$$F_{\mathrm{Rog}}^{T}I_{\mathrm{SoI}}=I_{\mathrm{Rog}},\ F_{\mathrm{halo}}^{T}I_{\mathrm{SoI}}=I_{\mathrm{halo}}$$

where L_{SoI}, R_{SoI}, F_{Rog}, F_{halo} are suitable matrices defined in [13], ϕ_{Rog}, ϕ_{halo} are the electric potentials of the electrodes covering the straps and the first wall, and V_{ext} is the voltage induced in the SoI by the time variations of the magnetic field due to ‘external’ sources (namely, the CS/PF coils, the plasma and the vacuum vessel) which have been computed at STEP1.

This system of dynamical equations can be solved with standard implicit time stepping, hence computing the value of I_{SoI} at each time instant. For the example depicted in figure 5, the dimension of vector I_{SoI} is of the order of few hundreds and hence the computation of a few thousands time steps takes only a few minutes on a standard computer architecture.

2.2.2. EM loads reconstruction in the SoI. Once the current density in the SoI $\boldsymbol{J}_{\mathrm{SoI}}$ has been computed, the EM Lorentz force density acting on the SoI can be computed as:

$$\boldsymbol{f}_{\mathrm{SoI}}=\boldsymbol{J}_{\mathrm{SoI}}\times\boldsymbol{B}_{\mathrm{tot}}.$$

The total magnetic field B_{tot} is computed as the superposition of the contributions of all the sources:

$$\boldsymbol{B}_{\mathrm{tot}}=\boldsymbol{B}_{\mathrm{coils}}+\boldsymbol{B}_{\mathrm{plasma}}+\boldsymbol{B}_{\mathrm{VV}}+\boldsymbol{B}_{\mathrm{SoI}}+\boldsymbol{B}_{\mathrm{tor}}$$

where the contribution of CS/PF coils $\boldsymbol{B}_{\mathrm{coils}}$, of the plasma $\boldsymbol{B}_{\mathrm{plasma}}$ and of the vacuum vessel $\boldsymbol{B}_{\mathrm{VV}}$ have been computed at STEP1, the contribution of currents in the SoI $\boldsymbol{B}_{\mathrm{SoI}}$ can be computed by $\boldsymbol{J}_{\mathrm{SoI}}$ with Biot-Savart integral and the toroidal field $\boldsymbol{B}_{\mathrm{tor}}$ can be computed from the knowledge of the current flowing in each TF coil. In the present paper, an ideal $1/r$ spatial behaviour has been assumed for the toroidal field, i.e. not considering its possible ripple.

If needed, with suitable spatial integrals of the force density $\boldsymbol{f}_{\mathrm{SoI}}$ over the SoI, also net forces and moments can be easily computed.

3. Results

3.1. Input data

The input data of the EM reconstruction procedure described in the previous section are the magnetic measurements recalled above. Such measurements will be directly available from the experiments during ITER operation, but presently they have been produced by suitable independent integrated simulations. In particular, in this paper we use the results of the procedure described in [5, 6], resulting from the coupling of DINA simulations for the axisymmetric plasma evolution with CARIDDI 3D EM simulation for the computation of synthetic magnetic measurements. The same simulations will provide also the reference values of the EM loads, which can be used for comparison with the results of the reconstruction procedure. It should be noted that the level of geometrical details used for these reference simulations is rather coarse, coherently with what has been shown in figure 5, to allow a fair comparison. This means that the EM loads reported in this paper should be intended as indicative and should not be considered for design purposes. Of course, during experiments, these reference EM loads will not be available.

Alternative approaches are possible for recovering the synthetic magnetic measurements needed by the EM reconstruction procedure, like for instance: integrated CarMa0NL [14] simulations, able to provide self-consistent axisymmetric plasma evolution and 3D EM structures; integrated JOREK-CARIDDI [15] simulations, able to provide self-consistent 3D plasma evolution and 3D EM structures; EM simulations carried out with commercial codes like ANSYS [16].

Two disruptive events have been considered (figures 6 and 7), selected with the aim of being largely complementary, from the point of view of the direction of movement (one upwards VDE, one downwards VDE) and in terms of the Current Quench time (one fast CQ, one slow CQ). These two antipode events will be labelled as ‘VDE UP Fast’ and ‘VDE DW Slow’. The application of the EM reconstruction procedure to these two events is hence particularly challenging and arguably covers a rather wide range of disruption parameters.

3.2. Results of STEP 1 (EM identification)

The results of the plasma identification are reported in figures 8 and 9. Evidently, the proposed plasma identification works well for both events, despite their differences in time and

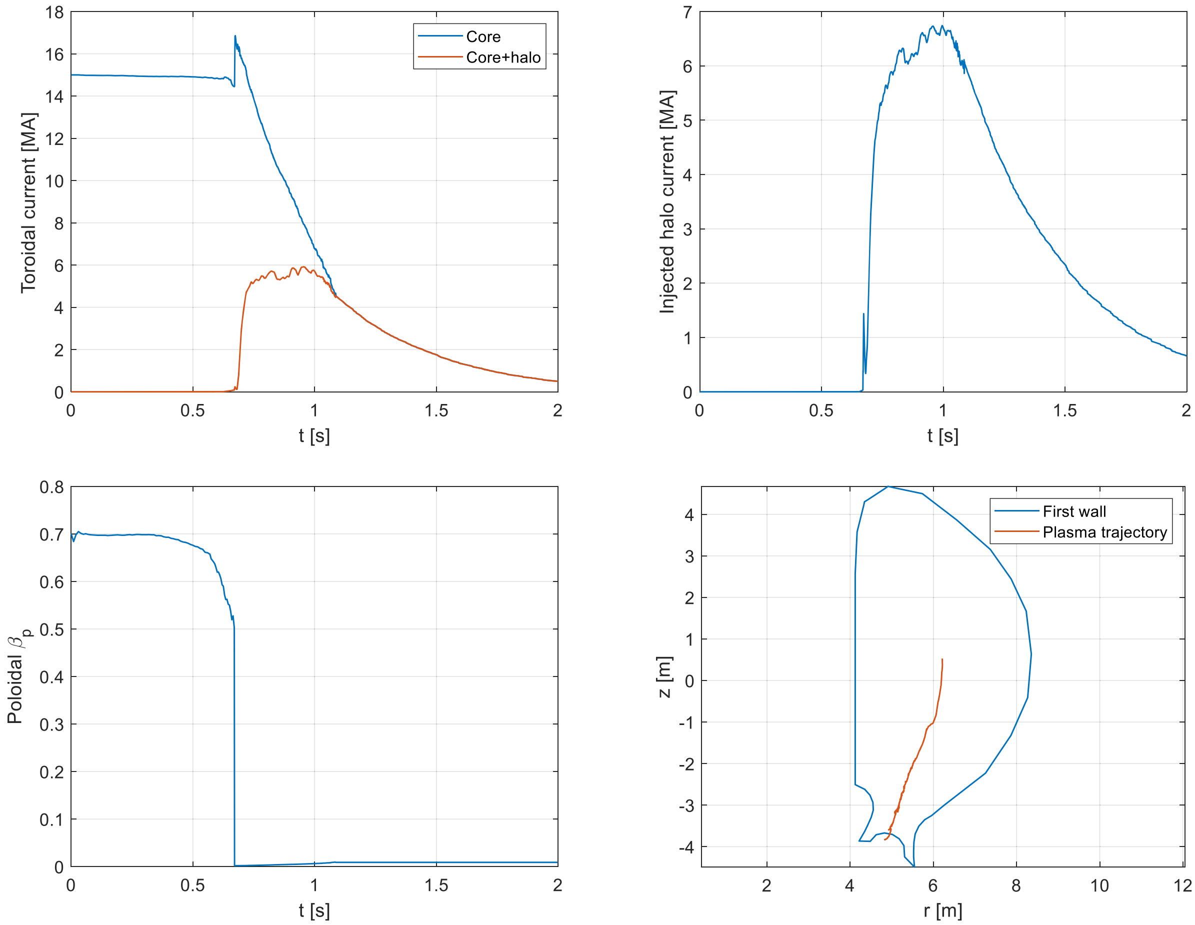

Figure 6. VDE DW Slow disruptive event: some plasma quantities.

spatial behaviour. In particular, the plasma current is very well approximated, thanks to the fact that blanket modules (which might improperly influence the results) do not carry a net toroidal current. The plasma centroid position is well approximated in the first phases of the event, when the error introduced by the currents flowing in the blanket modules is negligible. When such currents become significant, a discrepancy arise, especially in the VDE DW Slow event, during which the plasma-wall hitting point falls in the region of the blanket module#18 rather than in the divertor region. As we will show later, the practical consequences of this discrepancy are not very significant, since they happen in a time window in which the plasma current is low. It should also be noted that there is a systematic difference on the radial position, which is due to a different definition of the centroid radial position in DINA and in the EM reconstruction procedure.

The error introduced in the magnetic field, due to the approximation of the plasma current distribution with a small number of filaments, is quantified in figure 10. In this figure, we report the tangential magnetic field due only to plasma, at the spatial locations of discrete sensors AA shown in figure 2. In particular, we compare the reference value of the DINA computation with the approximate value computed using the small number of filaments chosen as detailed above.

For what concerns the identification of the vacuum vessel currents, figure 11 shows the comparison of the currents estimated in the vessel with the reference value of the DINA computation used to generate the synthetic magnetic measurements used as input to the procedure. The agreement is good and also the spatial distribution is consistent with physical expectations (figure 12).

It should be noted that the DINA computations are carried out using a description of the plasma current in terms of hundreds of filaments, carrying a current able to reproduce the details of the actual plasma current density distribution. Such level of details may not be available during operation, but nevertheless the good agreement showed in figures 10 and 11 confirms that even a simple representation of the plasma in terms of a small number of filaments may be adequate for the purposes of the present paper.

3.3. Results of STEP 2 (EM loads reconstruction)

The reconstructed EM loads are compared with the reference computations in figures 13 and 14, where the total force acting on various blanket modules are reported for the two disruptive events under analysis. The three components are referred to the normal and poloidally tangential directions with respect

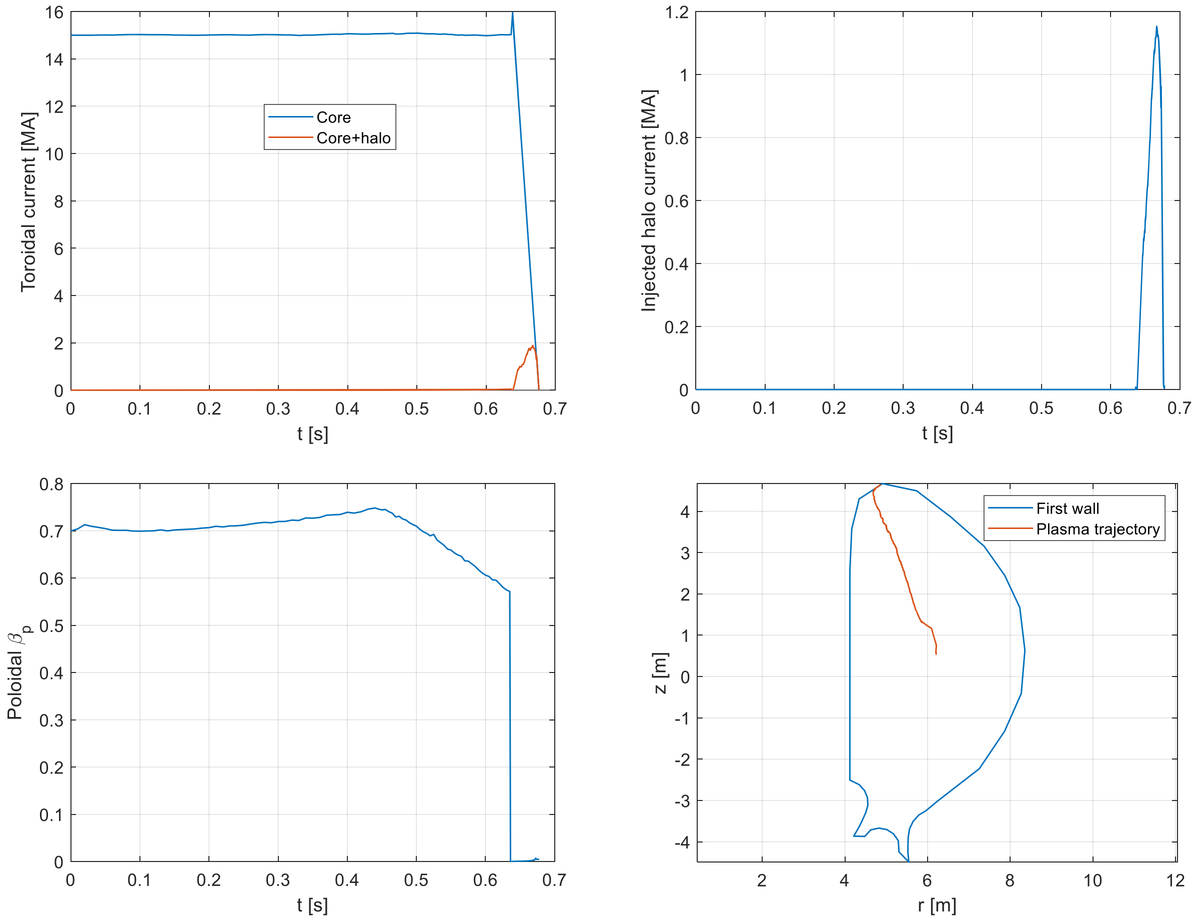

Figure 7. VDE UP Fast disruptive event: some plasma quantities.

to the first wall and to the toroidal direction. As mentioned before, the reference computations are carried out assuming a full knowledge and a detailed description of the plasma current density distribution, provided by DINA simulations. Hence, this positive comparison on EM loads includes the effect of the simplified description of the plasma in terms of a small number of filaments.

The agreement is generally very satisfactory, regardless the amplitude of the loads and the time scale for their occurrence, hence confirming the robustness of the reconstruction procedure. A few exceptions arise, which deserve a specific comment.

It can be noted that the agreement is in general very good for blankets not involved by halo currents injection (#6 and #10 for VDE DW Slow, #1 and #18 for VDE UP Fast). Conversely, the poorest agreement arise for some specific force components related to blanket modules in which the halo current has been injected, as for example for the normal force component for blanket modules #1 and #18 during VDE DW Slow. This component is in turn mostly due to the interaction of the poloidal component of the current density with the toroidal magnetic field. The poloidal current density in the blanket modules depends significantly on the assumptions made about the halo current spatial injection pattern. While the EM reconstruction procedure assumes a uniform distribution over the first wall, on the contrary the reference simulation features a very spatially localized halo current injection.

To check this conjecture, an additional VDE DW Slow simulation has been carried out with a different assumption on halo currents injection pattern (figure 15) and on the total injected halo current. In this new case, the halo current distribution is less spatially concentrated than in the reference case. Although still not uniformly distributed as in the EM reconstruction procedure, nevertheless the agreement on EM loads improves significantly (figure 16), hence confirming that the main source of discrepancy is indeed in the assumption about the injection of halo currents. The spikes present on blanket module#18 in the time window 1.2 s—1.3 s are due to the error in the plasma centroid reconstruction in the later phases of the disruption, when the plasma erroneously hits the wall at the location of blanket#18 instead of the divertor region.

4. Discussion

4.1. Robustness of the procedure

The robustness of the proposed EM reconstruction procedure has been successfully verified with a number of additional

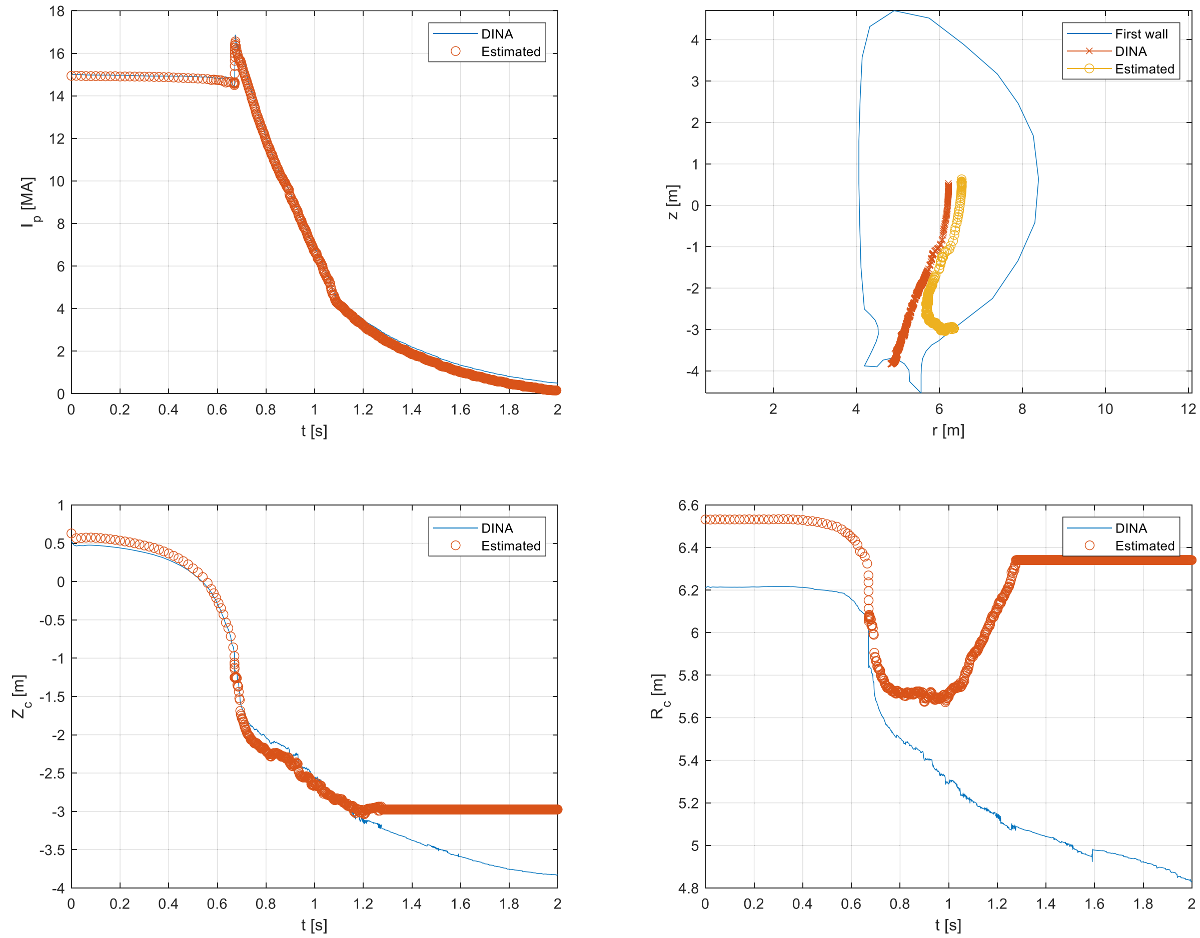

Figure 8. Results of the plasma identification for VDE DW Slow event.

tests, providing results quantitatively and qualitatively very similar to those presented in the previous section.

First of all, artificial noise has been added to the magnetic field measurements, as:

$$s_{\text{noise}} = s\ (1 + n_s) + n_0 t$$

where s is the ideal (noiseless) measurements and the quantities n_s, n_0 have a Gaussian distribution with zero mean and a standard deviation on which pessimistic assumptions have been made with respect to available estimates. The results show that the EM reconstruction procedure is robust with respect to the introduction of noise on measurements.

The robustness of the procedure to the failure of sensors has been successfully tested as follows. We have purposedly forced to zero the value of a random 1% of magnetic sensors, mimicking a very unlikely and pessimistic situation in which a number of magnetic sensors are failing simultaneously, but their measurements are used in the procedure assuming instead that they are working normally. The total estimated current flowing in the vacuum vessel changes between 1% and 2% in the cases analysed. This proves the robustness of the proposed procedure also to this kind of events.

As mentioned above, it should be noted that the proposed procedure is able to reconstruct all EM loads acting on components, i.e. not only the resulting forces reported extensively in section 3, but also moments, which are particularly important for some specific mechanical analyses, since they define mechanical stresses in the attachments of the components to the vessel. The robustness of the procedure has been tested also positively comparing the reconstructed moments with reference moments. Figure 17 shows an example for blanket module#6 for the two events considered; moments have been computed with respect to the barycentre of each component.

Also, the EM loads have been reconstructed also on other components—namely, the divertor structure. In this case, it has been shown that a satisfactory agreement can be obtained if Rogowski coils are placed not only around the straps connecting the divertor cassette, but also around the electrical connections of the cassette with the targets and the dome. This way, it is possible to identify correctly the spatial pattern of the injected halo currents along the various components and to reconstruct the corresponding EM loads.

4.2. Possible improvements

The proposed EM reconstruction procedure is highly modular, consisting of several different independent modules, each feeding the following with the data needed to proceed further, as shown in figure 1. Hence, each module can be in principle replaced by another computational

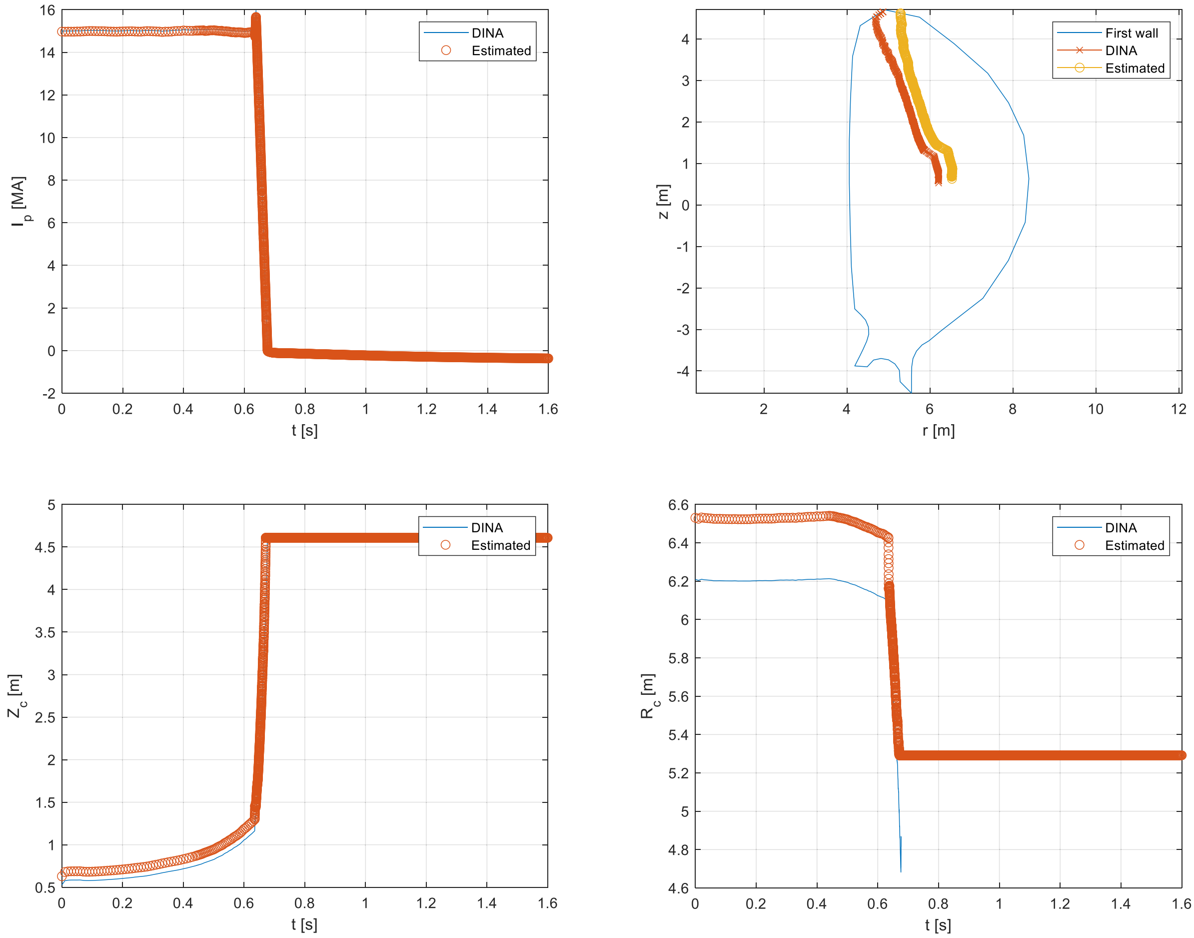

Figure 9. Results of the plasma identification for VDE UP Fast event.

tool, performing the same task with higher performances. Moreover, the EM reconstruction procedure is fully self-consistent in its present version, making simple but effective assumptions whenever the required information are not explicitly accessible; however, it is easy to incorporate additional information coming from other systems, if and when available.

Here follow a few non-exhaustive examples of possible improvements of the procedure.

- The plasma current and centroid identification can be replaced by other more sophisticated tools, like for instance those used in present-day devices for the real-time identification of plasma position and shape for control purposes [17, 18], those based on best fitting of magnetic measurements [19–21], or those based on virtual casing principle [22]. It should be noted however that some of these tools may be not always reliable during disruptions.
- The static SVD-based identification of the vacuum vessel currents can be replaced by other approaches, like for instance a Kalman filter [23].
- Possible identification of the centroid position using non-magnetic measurements [24] can be incorporated in the procedure.
- Information about the current density distribution inside the plasma (e.g. from plasma tomography [25]) can be added to improve the magnetic description of the plasma, e.g. in terms of the number of filaments used to represent the plasma and their currents, in order to reproduce a more realistic plasma current density distribution.
- A correct assumption about the halo current injection pattern is crucial for the accuracy of the reconstructed EM load. If additional information are available about the spatial distribution of halo currents (for instance, coming from Langmuir probes [26]), they can be easily included in the procedure. A simpler approach, still based on the use of Rogowski coils only, might be to resort to a spatially interpolated halo current injection pattern in the poloidal direction, instead of a piecewise constant one.
- Three-dimensional magnetic field maps produced by TF coils including ripple (e.g. from dedicated 3D magnetostatic analyses [27]) can be used.
- A library of different models of the structures of interest can be built, giving to the operator the possibility of choosing the most suitable case by case, depending on the purpose of the analysis (e.g. reconstruction of EM loads on specific components or sub-components), the level of details required (e.g. local EM force density vs. global EM loads) and the time allotted for computation.

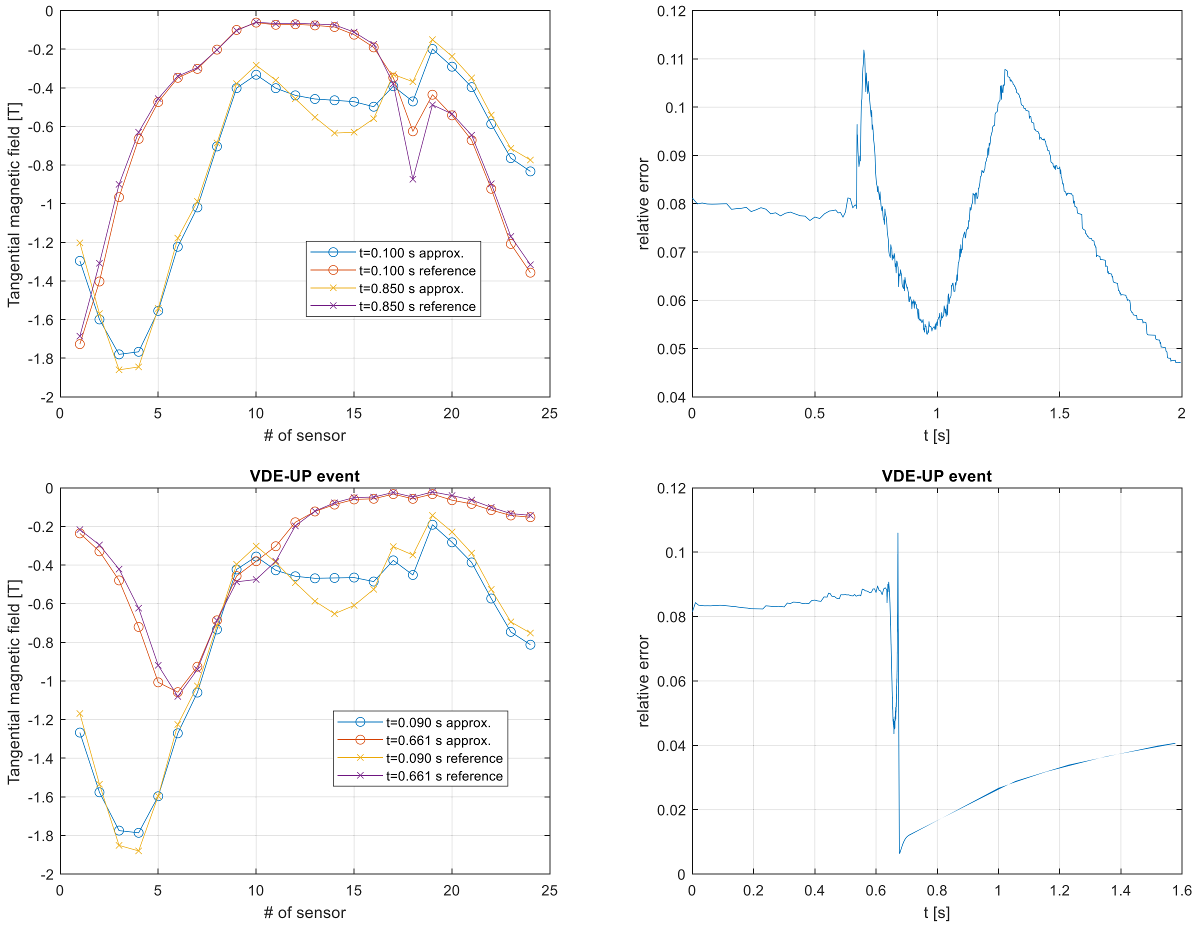

Figure 10. Comparison of tangential magnetic fields as measured by available sensors at two time instants (left) and relative error with respect to the norm of the vector of 24 measurements at first time instant (right).

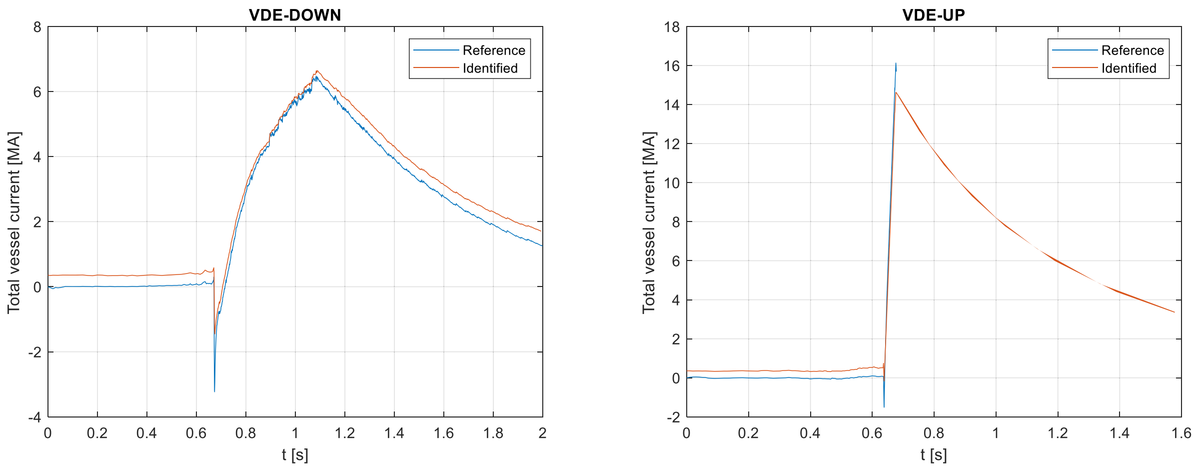

Figure 11. Results of the vacuum vessel current identification.

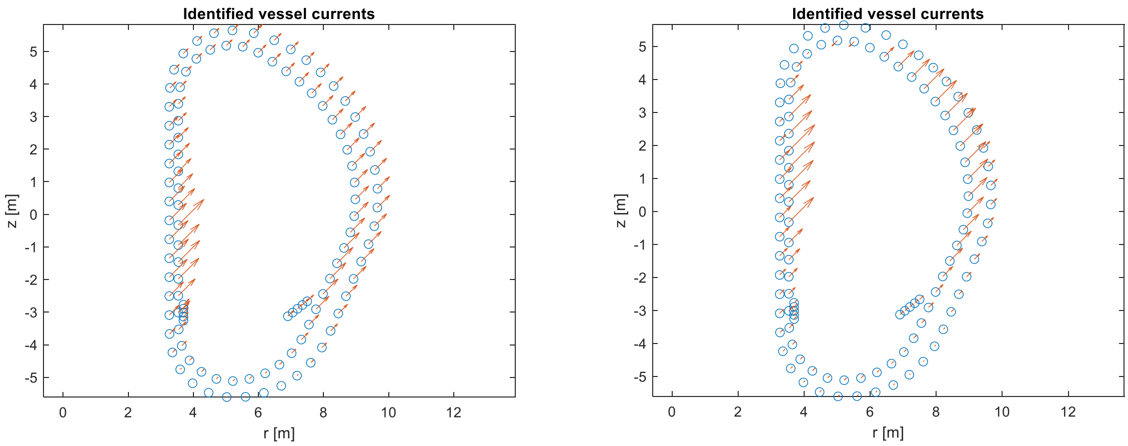

Figure 12. Sample spatial distribution of the identified vessel currents for VDE DW Slow (left) and VDE UP Fast (right).

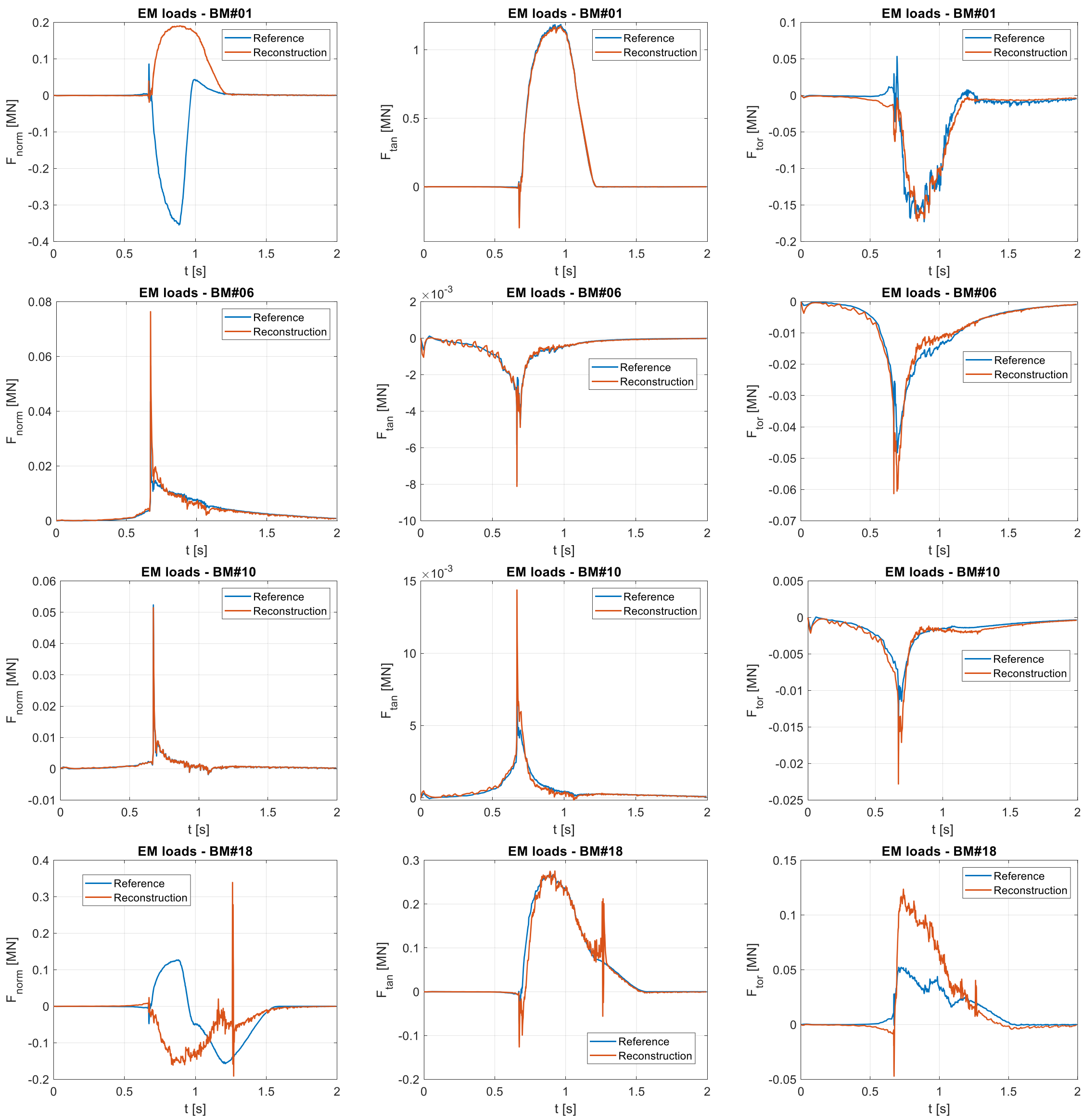

Figure 13. Comparison of reconstructed EM loads (components of total force acting on various blanket modules) with the reference computation for VDE DW Slow event.

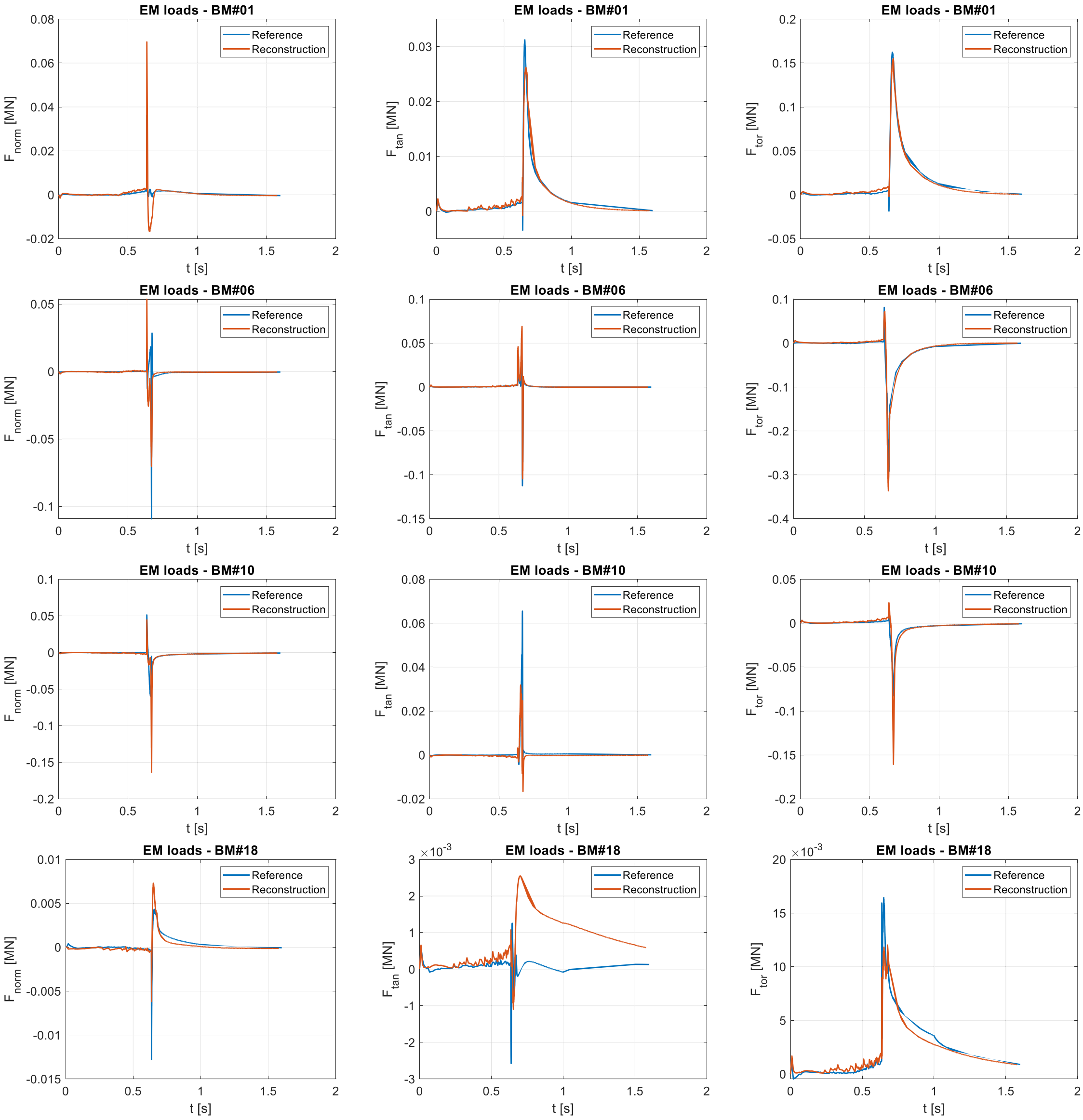

Figure 14. Comparison of reconstructed EM loads (components of total force acting on various blanket modules) with the reference computation for VDE UP Fast event.

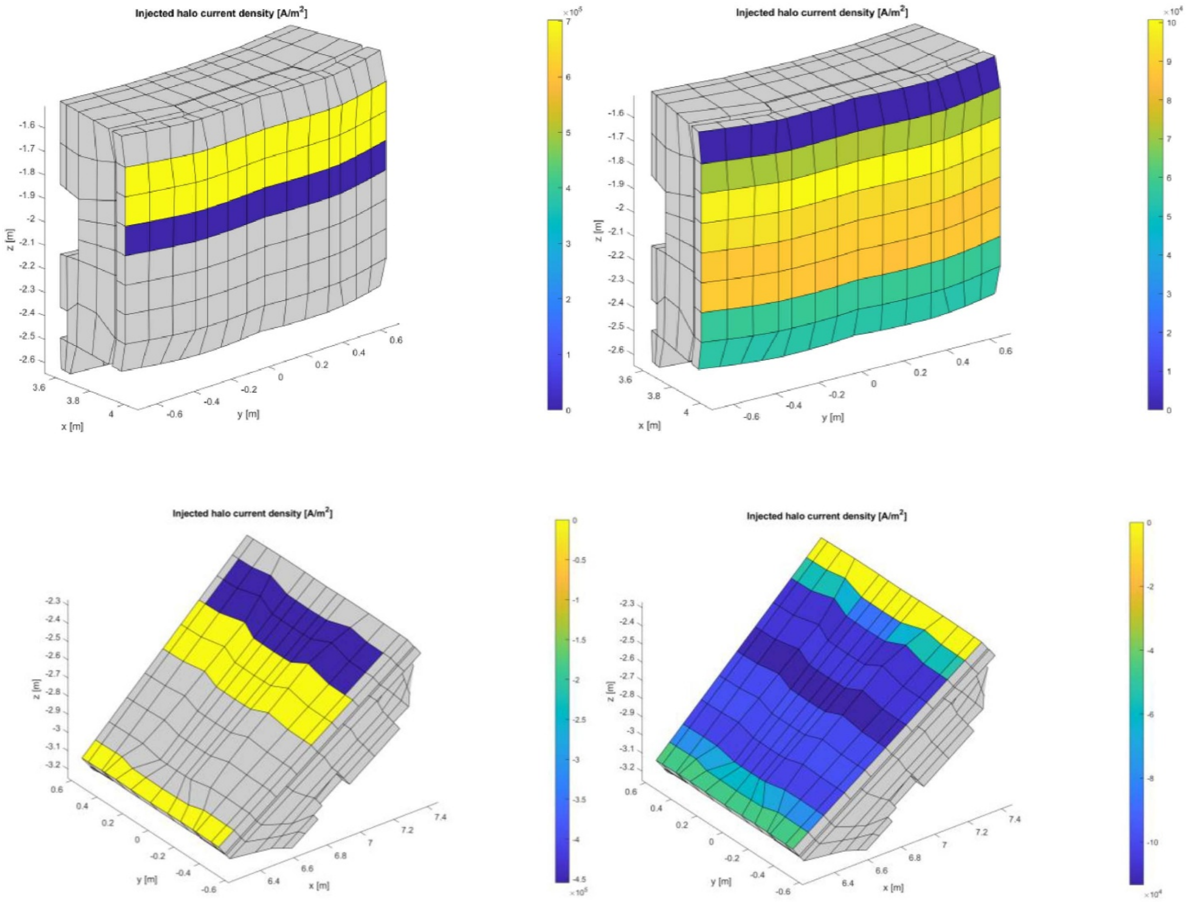

Figure 15. Halo current density injection pattern over blanket modules #1 and #18 in the reference (left) vs. additional (right) simulation.

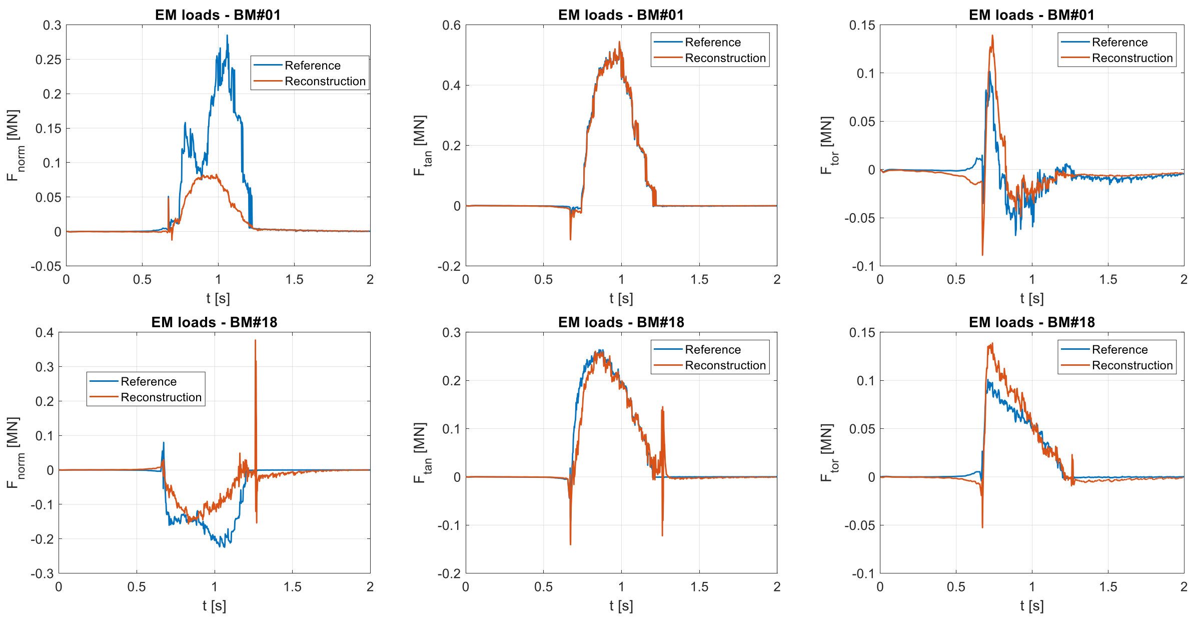

Figure 16. Comparison of reconstructed EM loads (components of total force acting on various blanket modules) with the additional computation for VDE DW Slow event.

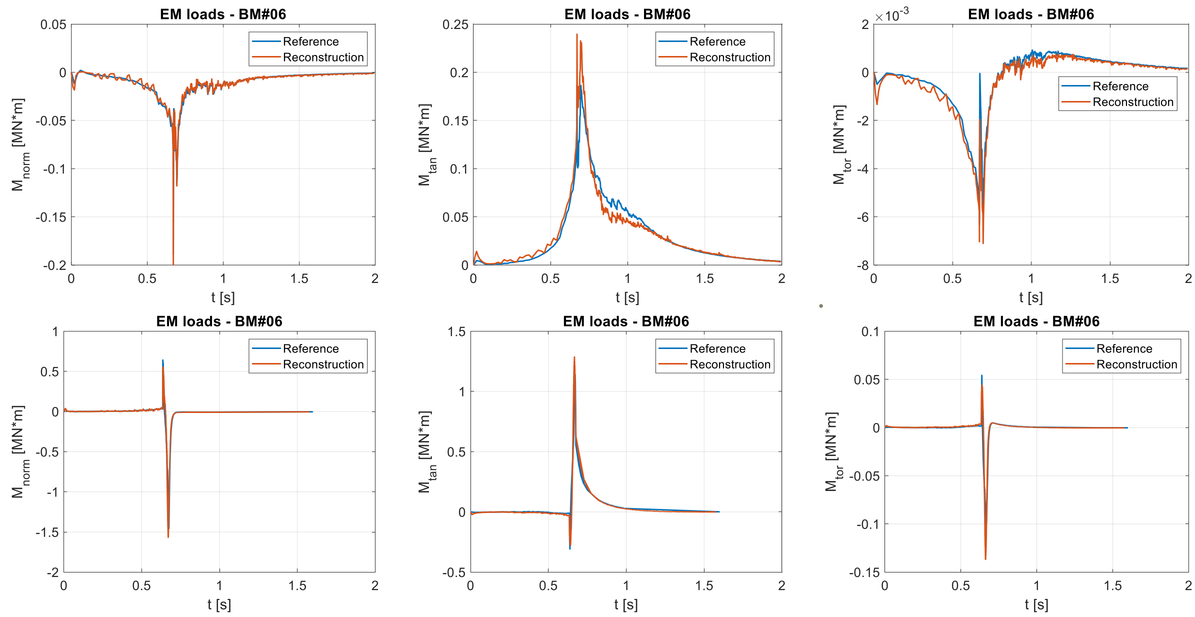

Figure 17. Comparison of reconstructed moments on blanket module#6 with reference computations: VDE-DOWN event (upper row), VDE-UP event (lower row).

5. Conclusions

In this paper we have presented the derivation of a two-step EM reconstruction procedure, able to reconstruct the EM loads on selected Structures of Interest, starting from magnetic measurements. The procedure has been successfully implemented for the ITER geometry and applied to two disruptive events. The same procedure can be in principle applied also to other fusion devices, provided that the required diagnostics is available.

The proposed EM reconstruction procedure satisfies all the desirable high-level requirements, namely:

- Only magnetic measurements are used as inputs
- The procedure can be run intershot
- The procedure is modular and flexible
- Additional information can be easily incorporated
- The procedure can adapt to available measurements

The reconstructed EM loads are generally in good agreement with the reference values; the causes of occasional discrepancies have been understood and have been mitigated whenever possible. One key finding is that the assumptions made on halo current spatial injection pattern may have a significant impact on the quality of the reconstruction of EM loads on specific components.

Future work will be addressed at the realization of a library of models with different levels of accuracy and at the application of the procedure to various cases of interest and to several structures, including the vacuum vessel. Specific attention will be given to the possibility of including further information in the EM reconstruction procedure and to a possible assessment with available experimental data. Once deployed, the results provided by this computational tool might potentially give a contribution also to a better understanding of some currently debated issues related to EM loads during disruptions, like for instance the role of the magnetic field penetration [28], the force generation after the disruption when the plasma current is zero [29], the role of the poloidal eddy currents [11, 12], the possible force reduction during mitigated disruptions due to the reduction of the vertical current moment [30].

Acknowledgment

This work was supported in part by Consorzio CREATE and by Italian Ministry of University and Research under PRIN grant P2022KNM7B (CUP E53D23014670001). The views and opinions expressed herein do not necessarily reflect those of the ITER organization.

Appendix

Here, we detail how, from magnetic measurements, we can identify the plasma current and centroid position. We suppose to know the magnetic field and the magnetic flux difference at a number of discrete locations along a closed line γ, specifically:

- $B_{\tan,k}$: tangential magnetic field at k-th location
- $\Delta\psi_k$: magnetic flux per radian difference between two consecutive locations (k and $k+1$)
- r_k. z_k: poloidal position of the kth location
- dl_k: distance between two consecutive locations (k and $k+1$)

We call Ω_γ the portion of the poloidal plane closed by γ.

For what concerns the plasma current, using Ampère's law, we have:

$$\mu_0 I_p = \oint_\gamma \boldsymbol{B}\cdot\hat{\boldsymbol{t}}\, dl \approx \sum_k B_{\tan,k} dl_k$$

where $\hat{t} = \hat{i}_\varphi \times \hat{n}$ and $\hat{n}$ is the outward normal to the 'diagnostic' surface. For what concerns the plasma centroid vertical position, we have:

$$\begin{aligned}\mu_0\, z_p I_p &= \iint_{\Omega_\gamma} \mu_0 z\, \boldsymbol{J}\cdot\hat{\boldsymbol{\iota}}_\varphi\, dS = \iint_{\Omega_\gamma} z\,(\nabla\times\boldsymbol{B})\cdot\hat{\boldsymbol{\iota}}_\varphi\, dS\\ &= \iint_{\Omega_\gamma} (\nabla\times z\boldsymbol{B})\cdot\hat{\boldsymbol{\iota}}_\varphi\, dS - \iint_{\Omega_\gamma} (\nabla z\times\boldsymbol{B})\cdot\hat{\boldsymbol{\iota}}_\varphi\, dS\\ &= \oint_\gamma z\boldsymbol{B}\cdot\hat{\boldsymbol{t}}\, dl - \iint_{\Omega_\gamma} \boldsymbol{B}\cdot\hat{\boldsymbol{\iota}}_r dS.\end{aligned}$$

The line integral at the R.H.S. is approximated by

$$\oint_\gamma z\,\boldsymbol{B}\cdot\hat{\boldsymbol{t}}\, dl \approx \sum_k z_k B_{tan,k} dl_k.$$

The additional term at the R.H.S. can be reduced similarly to a line integral and approximated according to the available diagnostics:

$$\begin{aligned}-\iint_{\Omega_\gamma} \boldsymbol{B}\cdot\hat{\boldsymbol{\iota}}_r dS &= -\iint_{\Omega_\gamma} \frac{\nabla\psi\times\hat{\boldsymbol{\iota}}_\varphi}{r}\cdot\hat{\boldsymbol{\iota}}_r dS = \iint_{\Omega_\gamma} (\nabla\psi\times\nabla\ln(r))\cdot\hat{\boldsymbol{\iota}}_\varphi\, dS\\ &= -\iint_{\Omega_\gamma} \nabla\times(\ln(r)\nabla\psi)\cdot\hat{\boldsymbol{\iota}}_\varphi\, dS\\ &= -\oint_\gamma \ln(r)\nabla\psi\cdot\hat{\boldsymbol{t}}\, dl \approx -\sum_k \ln(r_k)\Delta\psi_k.\end{aligned}$$

For what concerns the plasma centroid radial position, we have:

$$\begin{aligned}\mu_0\, r_p^2 I_p &= \iint_{\Omega_\gamma} \mu_0 r^2\, \boldsymbol{J}\cdot\hat{\boldsymbol{\iota}}_\varphi\, dS = \iint_{\Omega_\gamma} r^2\,(\nabla\times\boldsymbol{B})\cdot\hat{\boldsymbol{\iota}}_\varphi\, dS\\ &= \iint_{\Omega_\gamma} (\nabla\times r^2\boldsymbol{B})\cdot\hat{\boldsymbol{\iota}}_\varphi\, dS - \iint_{\Omega_\gamma} (\nabla r^2\times\boldsymbol{B})\cdot\hat{\boldsymbol{\iota}}_\varphi\, dS\\ &= \oint_\gamma r^2\boldsymbol{B}\cdot\hat{\boldsymbol{t}}\, dl + 2\iint_{\Omega_\gamma} r\boldsymbol{B}\cdot\hat{\boldsymbol{\iota}}_z dS.\end{aligned}$$

The line integral at the R.H.S. is approximated by:

$$\oint_\gamma r^2\,\boldsymbol{B}\cdot\hat{\boldsymbol{t}}\, dl \approx \sum_k r_k^2\, B_{tan,k} dl_k.$$

The additional integral above the cross-section is

$$\begin{aligned}2\iint_{\Omega_\gamma} r\boldsymbol{B}\cdot\hat{\boldsymbol{\iota}}_z\, ds &= \iint_{\Omega_\gamma} r\frac{\nabla\psi\times\hat{\boldsymbol{\iota}}_\varphi}{r}\cdot\hat{\boldsymbol{\iota}}_z\, ds\\ &= -2\iint_{\Omega_\gamma} (\nabla\psi\times\nabla z)\cdot\hat{\boldsymbol{\iota}}_\varphi\, ds\\ &= 2\iint_{\Omega_\gamma} \nabla\times(z\nabla\psi)\cdot\hat{\boldsymbol{\iota}}_\varphi\, dS = 2\oint_\gamma z\nabla\psi\cdot\hat{\boldsymbol{t}}\, dl\\ &\approx 2\sum_k z_k\Delta\psi_k.\end{aligned}$$

These expressions are coherent with [31], where the normal magnetic field is used instead of the poloidal flux differences.

ORCID iDs

Fabio Villone 0000-0003-4955-7988
Nicola Isernia 0000-0002-2121-3166
Guglielmo Rubinacci 0000-0003-0851-1035
Álvaro Yáñez-González 0000-0003-2450-1152

References

[1] Bandyopadhyay I. *et al* 2025 *Nucl. Fusion* **65** 103001
[2] de Vries P.C., Johnson M.F., Alper B., Buratti P., Hender T.C., Koslowski H.R. and Riccardo V. 2011 *Nucl. Fusion* **51** 053018
[3] Lehnen M. *et al* 2015 *J. Nucl. Mater.* **463** 39
[4] Maqueda L. *et al* 2023 *Fusion Eng. Des.* **188** 113435
[5] Sadakov S., Villone F., Rubinacci G. and Ventre S. 2022 *Plasma* **5** 306–23
[6] Sadakov S., Villone F., Iglesias D., Maqueda L., Almenara-Rescalvo J., Rubinacci G. and Ventre S. 2024 *Plasma* **7** 178–200
[7] Yanovskiy V.V. *et al* 2023 *49th EPS Conf. On Plasma Physics* (*Europhysics Conference Abstracts*) (*Bordeaux, France, 3–7 July 2023*) vol 47A p O2.104 (available at: lac913.epfl.ch/epsppd3/2023/html/Orals/O2_104_Yanovskiy.pdf)
[8] Pustovitov V.D. 2015 *Nucl. Fusion* **55** 113032
[9] Coutlis A., Bandyopadhyay I., Lister J.B., Vyas P., Albanese R., Limebeer D.J.N., Villone F. and Wainwright J.P. 1999 *Nucl. Fusion* **39** 663
[10] Sonato P., Miki N., Testoni P. and Zollino G. 2002 *Fusion Eng. Des.* **61–62** 415–22
[11] Yanovskiy V.V. *et al* 2019 *Fusion Eng. Des.* **146** 2338
[12] Isernia N., Pustovitov V.D., Villone F. and Yanovskiy V. 2019 *Plasma Phys. Control. Fusion* **61** 115003
[13] Albanese R. and Rubinacci G. 1998 *Adv. Imag. Electron. Phys.* **102** 1–86
[14] Villone F., Barbato L., Mastrostefano S. and Ventre S. 2013 *Plasma Phys. Control. Fusion* **55** 095008
[15] Isernia N., Schwarz N., Artola F.J., Ventre S., Hoelzl M., Rubinacci G. and Villone F. 2023 *Phys. Plasmas* **30** 113901
[16] Roccella R., Boccaccini L.V., Meyder R., Raff S. and Roccella M. 2008 *Fusion Eng. Des.* **83** 1212–6
[17] Anand H. *et al* 2024 *Nucl. Fusion* **64** 086051
[18] Moret J.-M., Duval B.P., Le H.B., Coda S., Felici F. and Reimerdes H. 2015 *Fusion Eng. Des.* **91** 1–15

[19] Swain D.W. and Neilson G.H. 1982 *Nucl. Fusion* **22** 1015
[20] Lao L.L., St. John H., Stambaugh R.D., Kellman A.G. and Pfeiffer W. 1985 *Nucl. Fusion* **25** 1611
[21] Luxon J.L. and Brown B.B. 1982 *Nucl. Fusion* **22** 813
[22] Malhotra D., Cerfon A.J., O'Neil M. and Toler E. 2020 *Plasma Phys. Control. Fusion* **62** 024004
[23] Huang Y., Mele A., Luo Z., Mattei M., Pironti A., Xiao B. and Yuan Q. 2022 *Nucl. Fusion* **62** 086010
[24] Santos J., Guimarãis L., Zilker M., Treutterer W. and Manso M. 2012 *Nucl. Fusion* **52** 032003
[25] Jardin A. *et al* 2024 *Plasma Phys. Control. Fusion* **66** 085010
[26] Adamek J. *et al* 2022 *Nucl. Fusion* **62** 086034
[27] Kripner L., Krbec J., Zelda J., Markovic T., Titus P., Vondracek P., Ficker O. and Hron M. 2023 *Fusion Eng. Des.* **187** 113378
[28] Pustovitov V.D., Rubinacci G. and Villone F. 2017 *Nucl. Fusion* **57** 126038
[29] Artola F.J., Loarte A., Hoelzl M., Lehnen M. and Schwarz N. (JOREK Team) 2022 *Nucl. Fusion* **62** 056023
[30] Schwarz N. *et al* 2023 *Nucl. Fusion* **63** 126016
[31] Braams B.J. 1991 *Plasma Phys. Control. Fusion* **33** 715